

1

2 **Supplementary Information for**

3 **Chaos in a simple model of a delta network**

4 **Gerard Salter, Vaughan R. Voller, Chris Paola**

5 **Gerard Salter**

6 **E-mail: gsalter@caltech.edu**

7 **This PDF file includes:**

8 Supplementary text

9 Figs. S1 to S8

10 Table S1

11 SI References

Supporting Information Text

Maximum Lyapunov Exponent Calculation. To calculate the maximum Lyapunov exponent (1), first, two simulations are started with an initial random separation d_0 , where the initial separation distance $|d_0|$ is very small. The simulations are run for a short time interval T_* , and the resulting separation d_1 is recorded. The second simulation is then reset along the d_1 separation vector such that the new separation distance equals $|d_0|$, and the procedure is repeated. As plotted in Figure S1, the quantity $\frac{1}{kT_*} \sum_{i=1}^k \ln \left(\frac{|d_i|}{|d_0|} \right)$, where k is the number of separations, is an estimate of the maximum Lyapunov exponent. As the number of steps k becomes large, the estimate of λ approaches the true value.

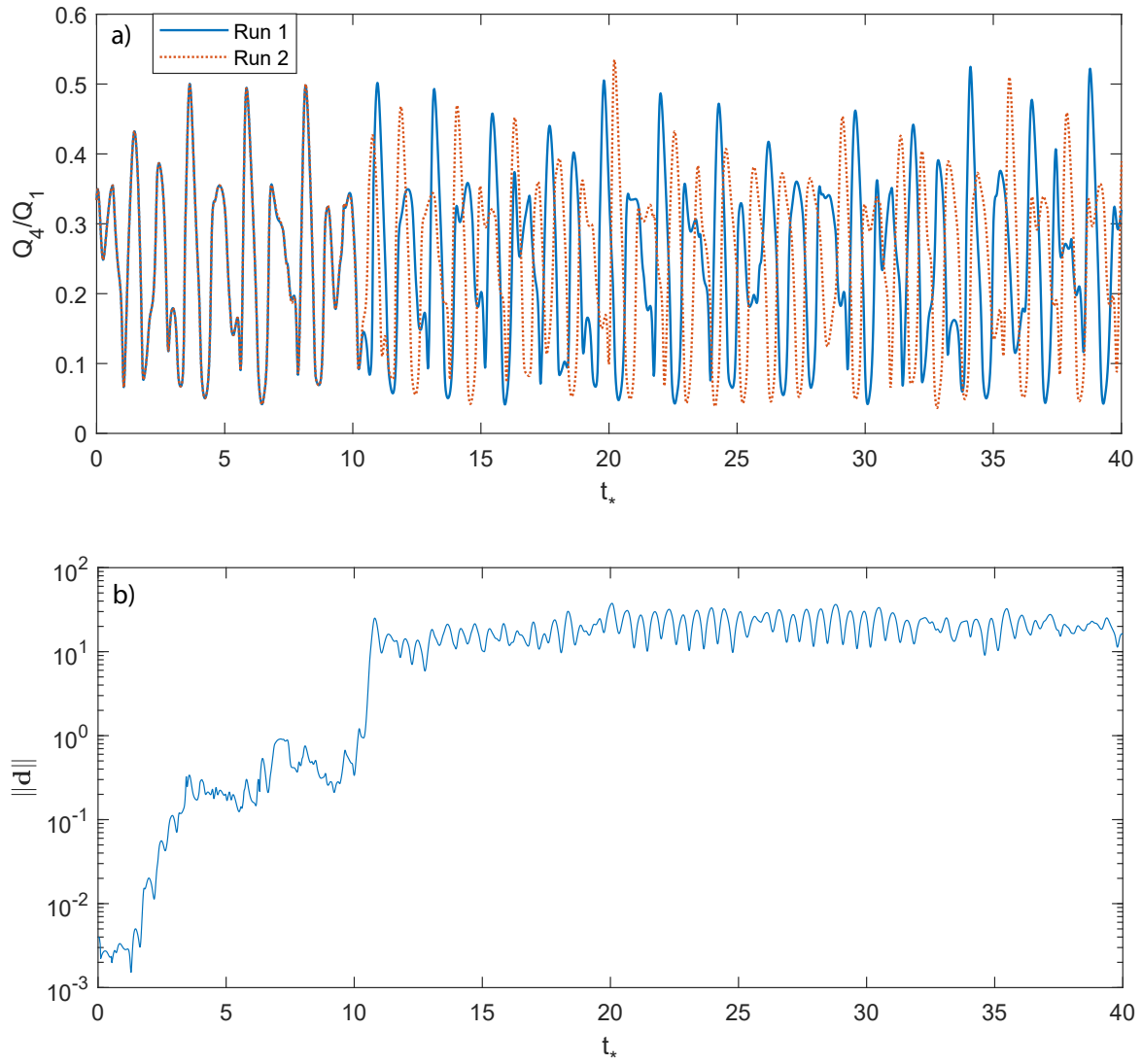


Fig. S1. Example of chaos within the soft avulsion regime. Run parameters listed in Table S1. a) Time series of two simulations started with similar initial conditions. b) Trajectories diverge exponentially until reaching maximum separation.

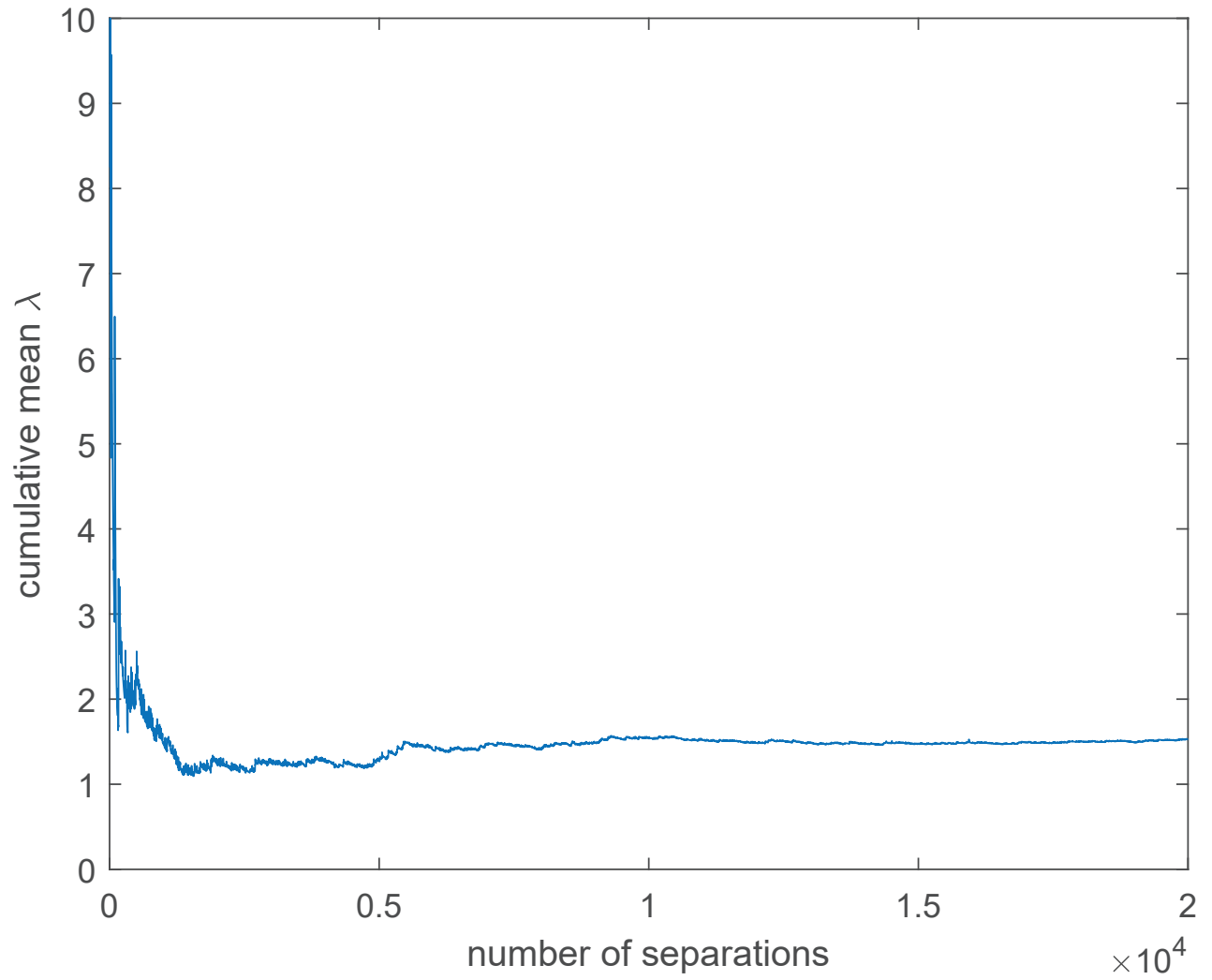


Fig. S2. Estimate of the maximum Lyapunov exponent λ using run parameters from Figures 3 and 4 of the main paper. An initial separation distance of $|d_0| = 2 * 10^{-7}$ is used, and the time interval for each separation is $T_* = 0.016$. We obtain a final value of $\lambda = 1.53$.

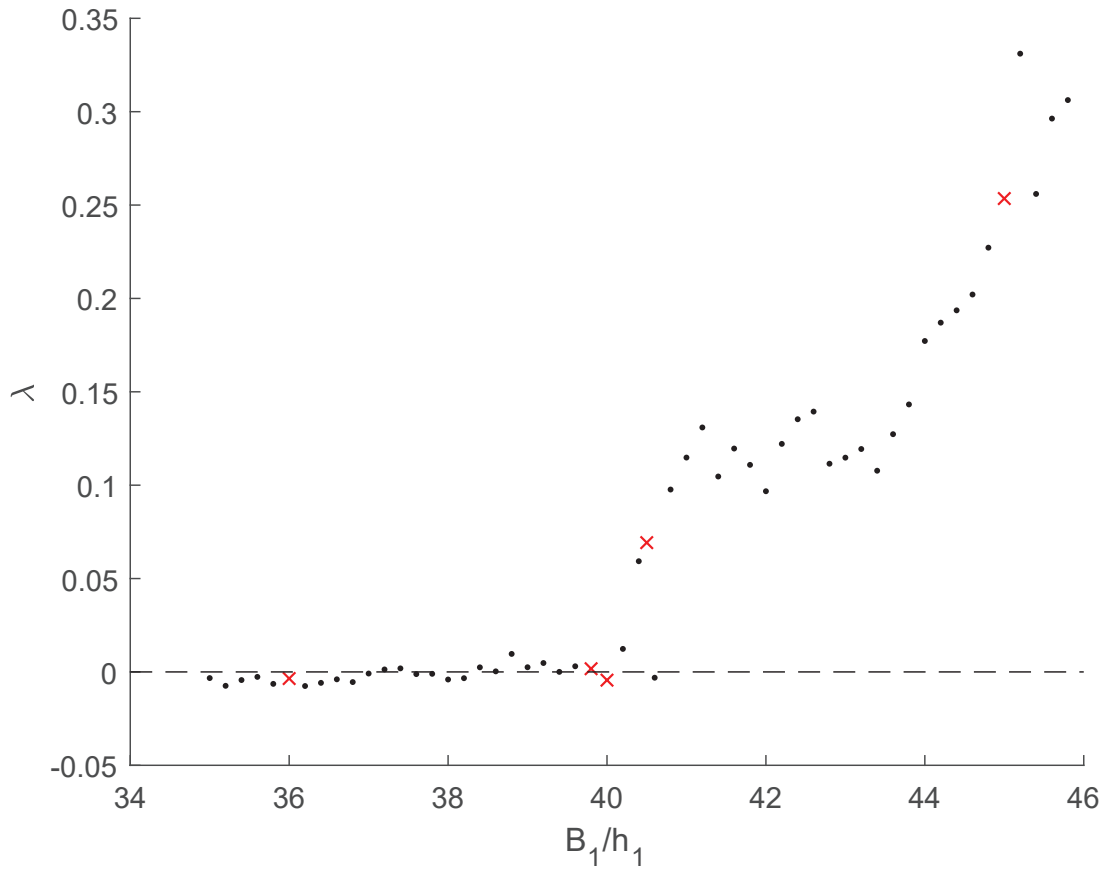


Fig. S3. Maximum Lyapunov exponent as a function of upstream channel aspect ratio B_1/h_1 . All other model parameters are the same as in Figure 2 of the main paper. Simulations shown in Figure 2 are plotted in red. Slight deviations from $\lambda = 0$ for periodic and quasiperiodic simulations are due to insufficient averaging times. Positive values of λ indicate chaos. An initial separation distance of $|d_0| = 2 * 10^{-7}$ is used, and the time interval for each separation is $T_* = 0.016$. Each λ value is obtained after averaging over 5000 separations.

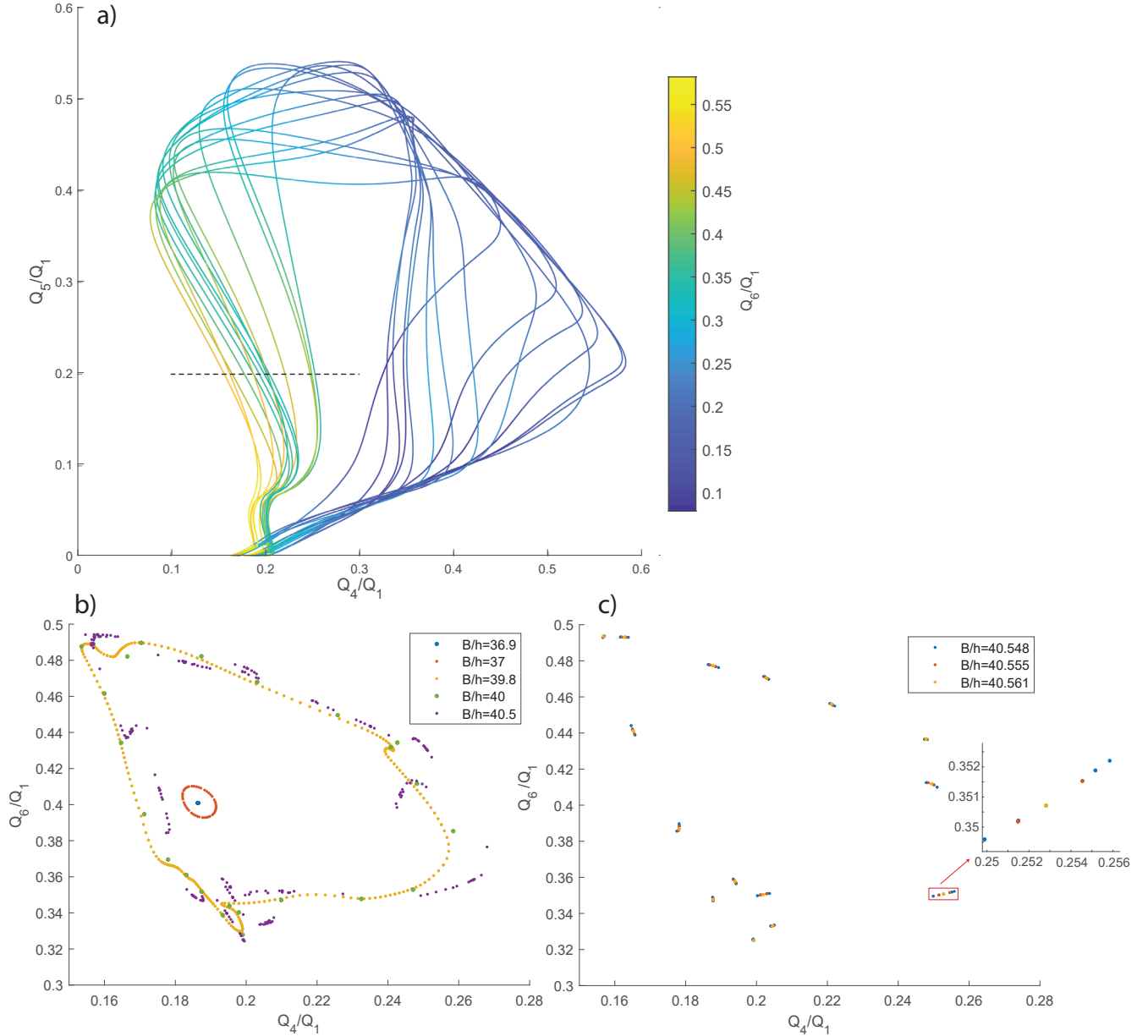


Fig. S4. a) Phase space plot of simulation with $B/h = 40.561$, all other parameters are the same as in Figure 2 of the main paper. The dashed line indicates the location of the Poincaré sections shown in subfigures b and c. b) Poincaré sections for different values of the aspect ratio. $B/h = 36.9$ corresponds to a period-one limit cycle. As the aspect ratio is increased, the solution becomes quasi-periodic ($B/h = 37$), which appears as a ring in the Poincaré section (a cross section through a 2-torus). This ring grows in size as aspect ratio is increased ($B/h = 39.8$). At $B/h = 40$ the solution is periodic rather than quasiperiodic, with 24 crossings of the Poincaré section. Finally, at $B/h = 40.5$, the solution is chaotic. The Poincaré sections illustrate the difference in shape between the quasiperiodic and chaotic attractors; the former produces a more even spacing of points over the surface of the 2-torus, whereas the latter has a fractal structure. c) Poincaré sections illustrating a period-doubling sequence. At $B/h = 40.561$ the solution is a limit cycle, with 15 crossings of the Poincaré section. Each crossing splits into two at $B/h = 40.555$ and then again at $B/h = 40.548$, illustrating period doubling. The inset plot is a zoomed in view of the region within the red rectangle.

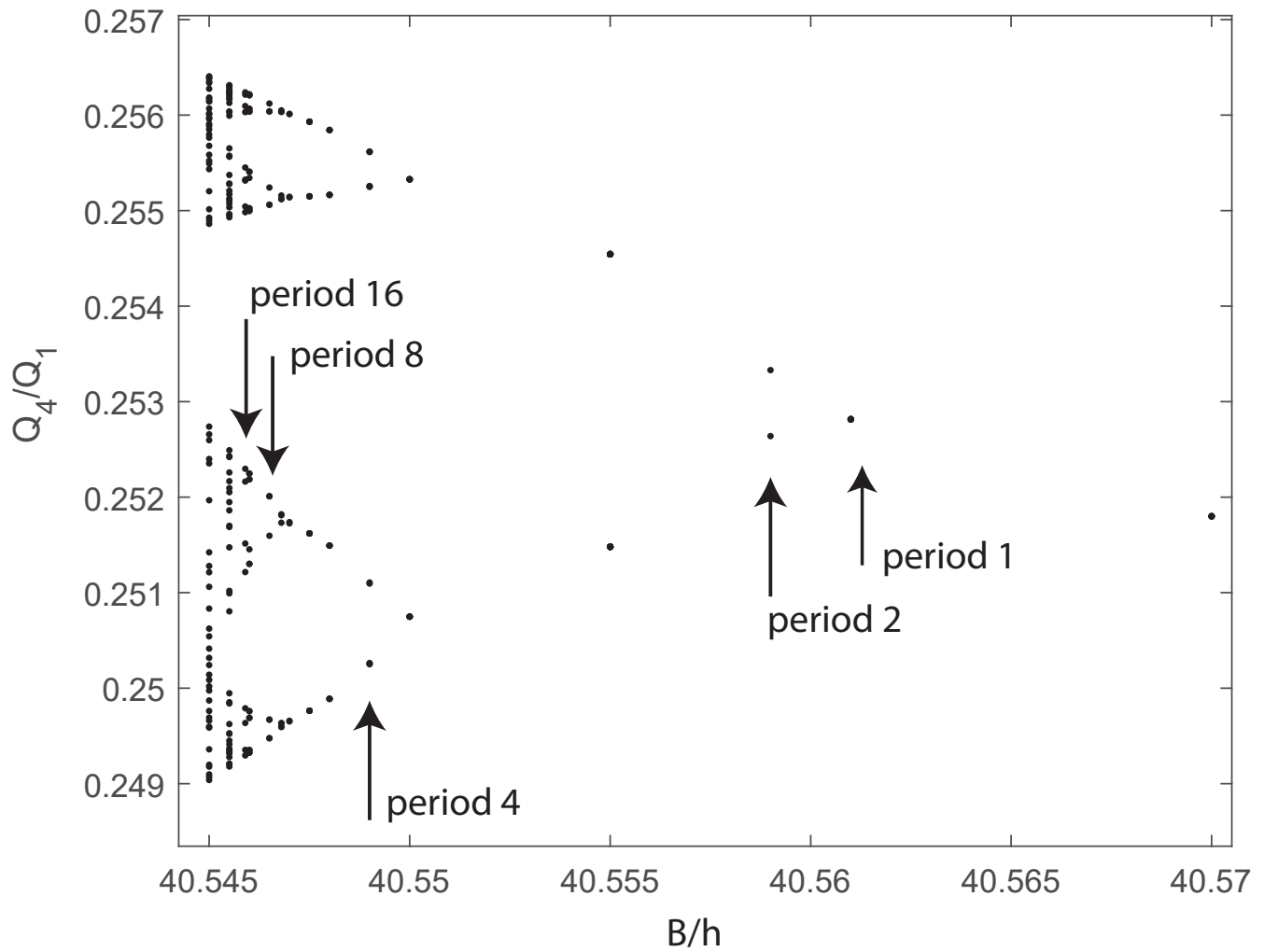


Fig. S5. Bifurcation diagram illustrating a period-doubling route to chaos. B/h acts as the control parameter and is plotted on the x-axis. As the control parameter is decreased, the figure shows a series of period doublings until the solution becomes chaotic at around $B/h = 40.5455$. The y-axis parameter is the Q_4/Q_1 value obtained from the Poincare section in Figure S4, for the region indicated by the red rectangle shown in subfigure c (a similar plot could be generated for any of the other fifteen crossings of the Poincare section). The locations of the period doubling bifurcations appear to be consistent with the Feigenbaum ratio, as has been shown in many other systems such as the logistic map and the Lorenz system.

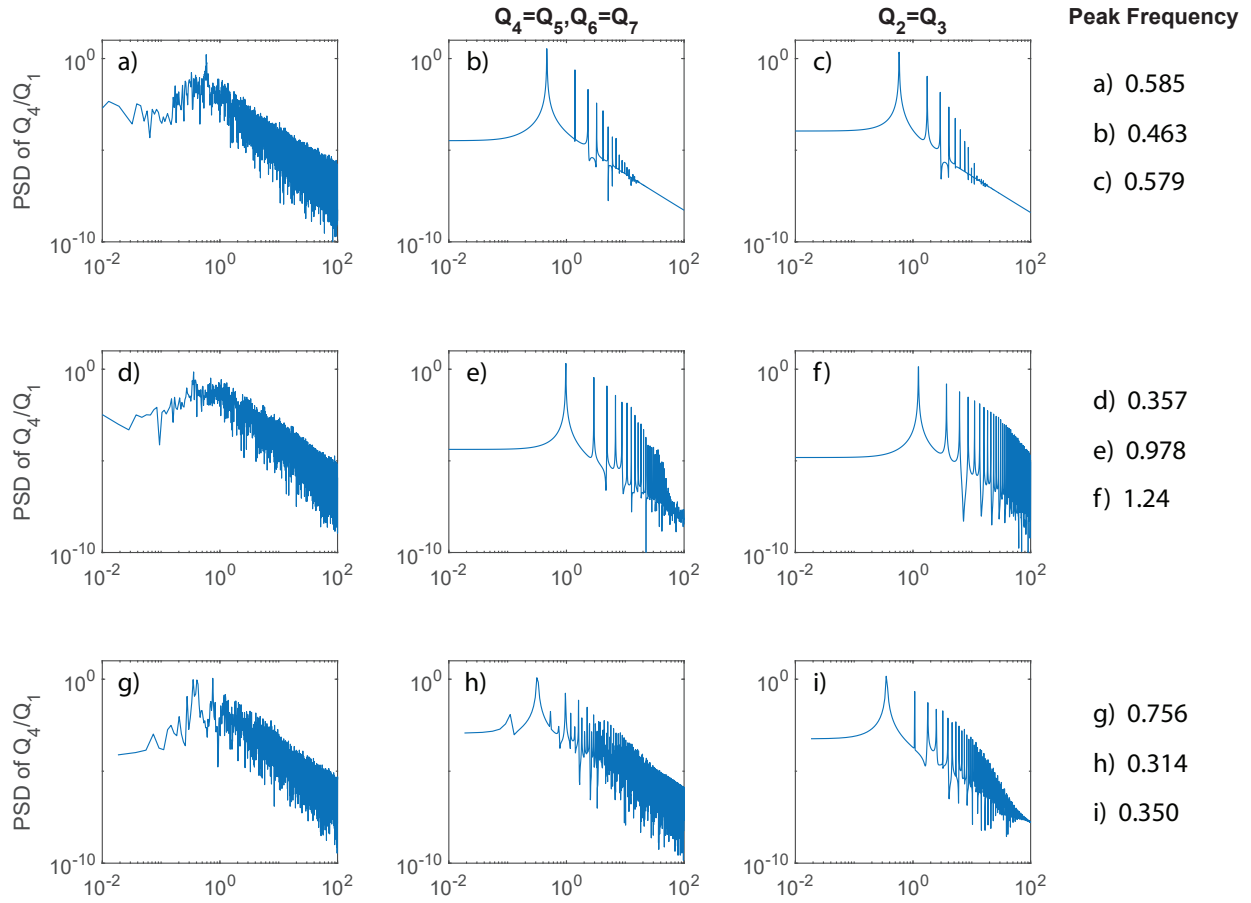


Fig. S6. Examples of the power spectra of time series generated with the model. Each row represents a different set of run parameters, listed in Table S1. The first column represents the full model with chaotic time series. The second column shows the power spectra when the downstream bifurcations are unperturbed and hence remain symmetric. The third column shows the power spectra when the upstream bifurcation is unperturbed.

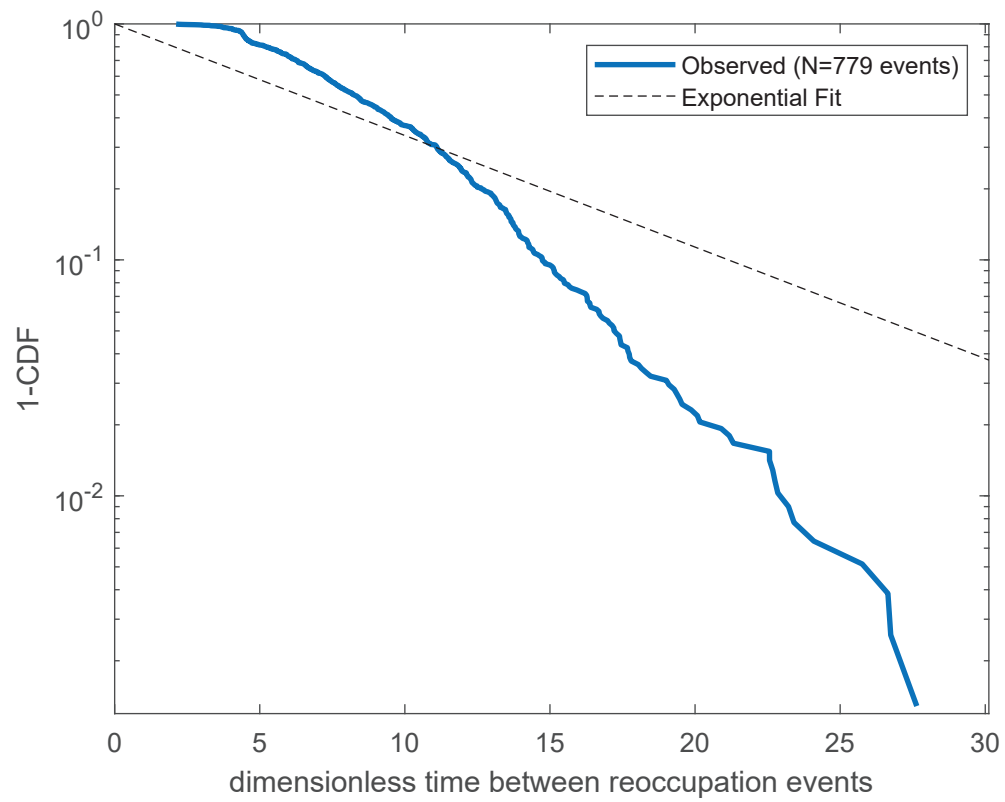


Fig. S7. Complementary cumulative distribution function of dimensionless time between reoccupation events (defined as moments when the discharge in a selected downstream branch goes from zero to nonzero). Parameter values are the same as in Figure 3 of the main paper. An exponential fit, corresponding to random, independent events, is shown for reference. In the simulation, both long and short waiting times are rare compared to random.

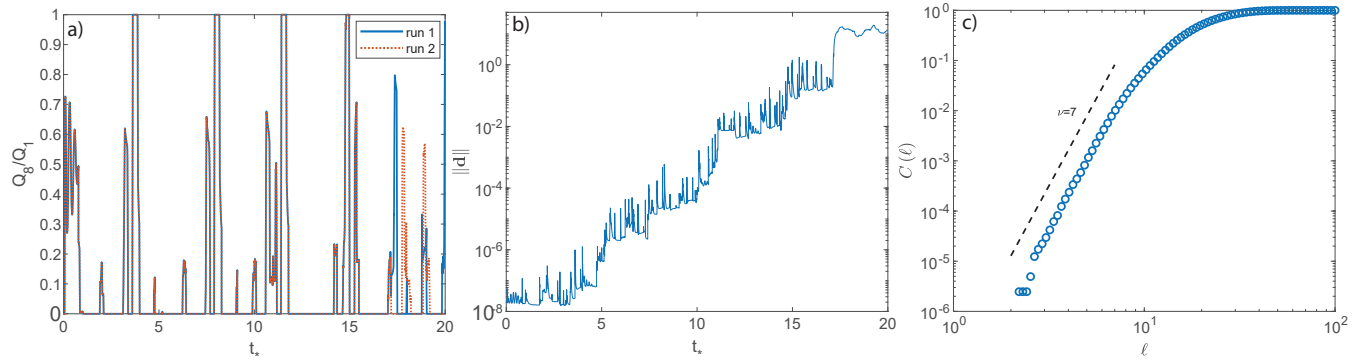


Fig. S8. Simulation with network geometry consisting of three orders of bifurcations (eight outlets). Branch widths from upstream to downstream are 0.7, 0.5, and 0.35 times the upstream branch width. All other model parameters are listed in Table S1. a) Discharge time series in one of the eight downstream branches for two simulations with nearly identical initial conditions. b) Separation distance between the two simulations from the previous subfigure as a function of time, showing exponential divergence. c) Plot of the correlation integral, indicating a fractal dimension of approximately $\nu = 7$.

Table S1. Model run parameters for Figures S1,S3, and S8.

| Figure | Fig. S1 | Fig. S3 a-c | Fig. S3 d-f | Fig. S3 g-i | Fig. S8 |
|--------------|-----------|-------------|-------------|-------------|-----------|
| B_1/h_1 | 30 | 100 | 100 | 100 | 100 |
| τ_{*1} | 0.08 | 1 | 0.06 | 1 | 0.06 |
| S_1 | 10^{-3} | 10^{-3} | 10^{-3} | 10^{-3} | 10^{-3} |
| F | 0 | 0.427 | 0.6887 | 0.7099 | 0.7 |
| L_1/B_1 | 18 | 18 | 18 | 18 | 18 |
| L_2/B_4 | 30 | 30 | 30 | 96 | 33 |
| L_4/B_4 | 240 | 156 | 66 | 186 | 36 |
| L_8/B_8 | N/A | N/A | N/A | N/A | 90 |
| α | 3 | 3 | 3 | 3 | 3 |
| r | 0.5 | 0.5 | 0.5 | 0.5 | 0.5 |
| m | 1.5 | 2.5 | 1.5 | 2.5 | 1.5 |
| τ_{*cr} | 0.047 | 0 | 0.047 | 0 | 0.047 |

References

1. M Casartelli, E Diana, L Galgani, A Scotti, Numerical computations on a stochastic parameter related to the kolmogorov entropy. *Phys. Rev. A* **13**, 1921 (1976).